Available online at www.sciencedirect.com

SciVerse ScienceDirect

Ceramics International 39 (2013) 3669–3676

CERAMICS INTERNATIONAL

www.elsevier.com/locate/ceramint

Structural, electrical and optical properties of molybdenum-doped TiO_2 thin films

Boen Houng*, Cheng Chiu Liu, Min Tai Hung

Department of Materials Science and Engineering, I-Shou University, Kaohsiung City 840, Taiwan, Republic of China

Received 12 September 2012; received in revised form 12 October 2012; accepted 12 October 2012
Available online 23 October 2012

Abstract

Molybdenum doped TiO_2 (MTO) thin films were prepared by radio frequency (RF) magnetron sputtering at room temperature and followed by a heat treatment in a reductive atmosphere containing 90% N_2 and 10% H_2. XRD and FESEM were employed to evaluate the microstructure of the MTO films, revealing that the addition of molybdenum enhances the crystallization and increases the grain size of TiO_2 films. The optimal electrical properties of the MTO films were obtained with 3 wt% Mo doping, producing a resistivity of $1.1 \times 10^{-3}\,\Omega\,cm$, a carrier density of $9.7 \times 10^{20}\,cm^{-3}$ and a mobility of $5.9\,cm^2/Vs$. The refractive index and extinction coefficient of MTO films were also measured as a function of film porosity. The optical band gap of the MTO films ranged from 3.28 to 3.36 eV, which is greater than that of the un-doped TiO_2 film. This blue shift of approximately 0.14 eV was attributed to the Burstein–Moss effect.

Keywords: TiO_2 film; RF sputtering; Optical band gap; Burstein–Moss

1. Introduction

Transparent conducting oxide films (TCOs) are electrically conductive and optically transparent in thin layers. Doped single-cation oxide films such as In_2O_3 and SnO_2 have been employed in technological applications for over 50 years. The wide range of applications for transparent conducting oxide films in electronic devices has generated interest in understanding the growth and characterization of these materials. These applications include flat-panel displays, low-emissivity windows, solar cells, electrochromic devices, electromagnetic-shielding coatings, antennas for cars and radar protection for fighter planes, and heated windows [1–4].

To date, tin-doped indiumoxide (ITO) is the most successful TCO and is used as the industry standard because of its high light transmission in the visible range, high infrared reflection, and low electrical resistivity. However, ITO has the drawback of being expensive. Indium, the film's primary metal, is rare, and its price strongly depends on market demand [5]. In addition, many years of intense study have gone into improving the properties of ITO, including the application of new deposition techniques such as ion-beam-assisted deposition [6] or pulsed laser deposition [7], improvements in the crystal quality of ITO films [8,9], and the use of an ultra-high-density ITO target [10]. However, as shown in Fig. 1, the results of these efforts have not been promising [11].

Over the last few years, TiO_2 has gained increasing attention as a TCO material after a Nb-doped anatase TiO_2 film with excellent resistivity and transmittance, comparable to those of ITO, was produced by Furubayashi et al. [12]. The advantages of anatase TiO_2 as a TCO include its relative low effective mass, low cost and stability in a hydrogen plasma atmosphere which is used to produce solar cells. TiO_2 is a wide band gap oxide that occurs in three distinct polymorphs: rutile, anatase, and brookite. Un-doped anatase is an anisotropic, tetragonal insulator ($a=0.378$ nm and $c=0.952$ nm) with a band gap of 3.2 eV [13]. As shown in a previous study, an un-doped semiconducting TiO_2 thin film can be synthesized with an

*Corresponding author. Tel.: +886 76579708; fax: +886 76578444.
E-mail address: boyen@mail.isu.edu.tw (B. Houng).

0272-8842/$ - see front matter © 2012 Elsevier Ltd and Techna Group S.r.l. All rights reserved.
http://dx.doi.org/10.1016/j.ceramint.2012.10.197

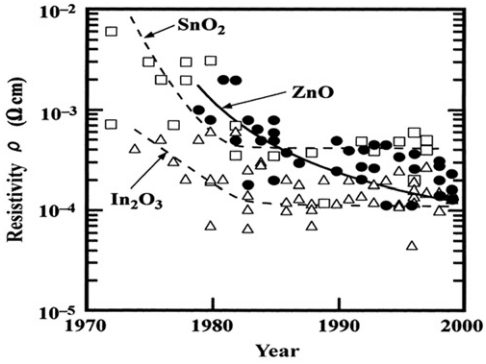

Fig. 1. Reported resistivities of binary transparent conducting oxide materials [11].

anatase structure on a $LaAlO_3$ substrate using reactive sputtering deposition. When water vapor was used as the oxidizing species, n-type semiconducting behavior was observed. The oxygen-deficient defects caused the metallic-like behavior. The corresponding electrical resistivity is approximately 0.2–3 Ω cm with a carrier concentration of $2–2.5 \times 10^{18}\ cm^{-3}$ and a mobility of 1–13 cm^2/Vs. TiO_2 can also be made into an n-type semiconductor with a carrier concentration of approximately $10^{19}\ cm^{-3}$ via impurity chemical substitution or the introduction of Ti interstitials [14–17]. Hitosugi et al. reported that polycrystalline Nb-doped anatase TiO_2 films fabricated on glass substrates by pulsed laser deposition (PLD) and then subjected to post-annealing in a pure H_2 atmosphere exhibited an electrical resistivity of 1.5×10^{-3} Ω cm and an optical transparency of approximately 60–80% [18]. More recently, research groups in Japan have reported that Nb-doped anatase TiO_2 films epitaxially grown on various single-crystal substrates using PLD, exhibit a low resistivity of approximately 3×10^{-4} Ω cm and a high transmittance of 95% in the visible region [19,20]. In addition to adding metal ion impurities into the TiO_2 lattice, post-annealing treatment, such as vacuum annealing [21,22] or annealing under a reductive atmosphere [23,24], has also been successful in enhancing the properties of TiO_2 thin films. An annealing under a reductive atmosphere, such as pure hydrogen, is a particularly attractive and effective treatment that can produce a resistivity of 10^{-4} Ω cm. However, relative to vacuum annealing, greater precautions and production costs are required, making this process impractical. The aim of this work is to investigate the properties of TiO_2 films doped with molybdenum under heat treatment in a reductive atmosphere of 90% N_2 and 10% H_2. The influence of the MoO_3 concentration on the microstructure, electrical and optical properties of TiO_2 thin films presented in this work.

2. Experimental procedure

Molybdenum-doped TiO_2 films were prepared by a RF magnetron sputter on glass substrate (Corning 1373) at room temperature. A mixture of TiO_2 (Aldrich, St. Louis, USA, 99.99%) and MoO_3 (Aldrich, St. Louis, USA, 99.99%) powders was sintered at 1200–1400 °C for 4 h as the target for later deposition. The MoO_3 doping concentrations varied from 1 to 10 wt%. The distance between the target and the substrate was 7 cm. The vacuum chamber was evacuated to a pressure of 10^{-6} Torr prior to deposition operation. The sputtering were performed at a gas pressure of 3 mTorr in a pure argon atmosphere, and the RF power was 100 W. The sputtering time was 90 min, producing a thickness of approximately 780 ± 15 nm. After sputtering, the films were annealed at 600 °C for 1 h in a mixing gas containing 90% N_2 and 10% H_2.

An X-ray diffractometer (Panalyical, X'pert Pro) with Cu Kα radiation ($\lambda = 0.1542$ nm) was used to evaluate the crystal structure. The surface microstructure and morphology of the films were characterized by field emission scanning electron microscopy (FESEM, Philips, XL-40FEG). The surface composition of the molybdenum-doped TiO_2 films were investigated using a VG ESCA spectrometer with an Mg Kα X-ray source ($hv = 1253.6$ eV). The pressure of the analyzer chamber was maintained at 5×10^{-8} Pa. Spectra were calibrated with respect to the C 1s peak at 284.6 eV. The resistivity was measured with the Van der Pauw method. Optical transmittance measurements were performed in 300–900 nm radiation using a UV/double-beam spectrophotometer. The wavelength dependent refractive indices and extinction coefficients of the Mo-doped TiO_2 films were measured by a variable angle spectroscopic ellipsometer (VASE, J.A. Woollan).

3. Microstructure characterization

The XRD patterns of the as-deposited samples do not show any peaks, including that the un-doped TiO_2 films were amorphous. Fig. 2 shows the X-ray diffraction

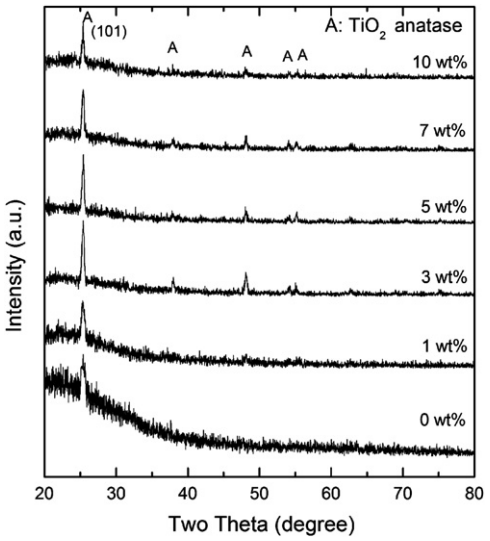

Fig. 2. X-ray diffraction patterns of un-doped TiO_2 film and TiO_2 films doped with 1–10 wt% Mo.

patterns of the MTO films sputtered at room temperature and annealed at 600 °C for 1 h with MoO_3 concentrations ranging from 0 to 10 wt%. According to the XRD patterns, all of the MTO films were composed of a well-crystallized anatase phase, which correspond well with the JCPDS data (file number 21-1272). No characteristic MoO_3 peaks were observed in the MTO thin films up to 10 wt%. This finding suggests the incorporation of Mo ions into the TiO_2 lattice. Moreover, (101) was the predominant plane for the films prepared using this method, indicating that the MTO films had a (101) preferentially oriented texture. The relative intensity of the (101) reflection increased with increasing Mo doping concentration up to 3 wt% and then gradually decreased. The particle size was evaluated using the full width at half maximum (FWHM) of the intense (101) diffraction peak of anatase TiO_2 according to the Scherrer equation:

$$D = 0.94\lambda / FWHM \cos\theta \quad (1)$$

where D is the particle size of the thin films, θ is the angle of the peak intensity and λ is the wavelength of the X-rays. The FWHM (in radians) is inversely proportional to the particle size and is related to the degree of crystallinity in polycrystalline thin films [25]. The results are given in Fig. 3. The average anatase particle size of the MTO films was greater than that of the un-doped TiO_2 films, suggesting that the addition of MoO_3 enhanced the crystallization of the TiO_2 thin films. The film doped with 3 wt% MoO_3 has the greatest particle size: approximately 32 nm.

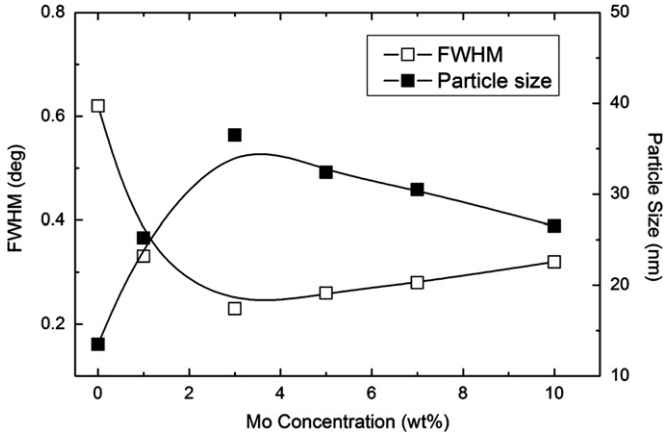

Fig. 3. FWHM and particle size of MTO films as a function of Mo doping concentration.

Fig. 4 shows the FESEM photomicrographs of un-doped TiO_2 and TiO_2 doped with 3 and 10 wt% MoO_3 annealed at 600 °C. All of the films exhibit a uniform surface without cracks. There is also a difference in the particle size between these films. The particles of un-doped TiO_2 films are very small, with an average size of approximately 16 nm. In contrast, the particles of the MTO films are larger, with an average particle size of approximately 35 nm for 3 wt% and 25 nm for 10 wt% MoO_3. These results are consistent and correlate well with those of XRD measurements.

To further confirm the chemical state and surface composition of MTO thin films, we performed X-ray photoemission spectroscopic (XPS) measurements. In Fig. 5, Mo 3d core levels are presented for MTO thin films with different Mo doping concentrations. Based on a fitting analysis using a Gausian/Lorentzian mixing function, a single doublet could not resolve the observed XPS spectra of the films. It was necessary to deconvolute the Mo 3d to estimate the Mo oxidation state distributed in the MTO films. The deconvolution yielded two doublets whose binding energies are almost constant regardless of Mo doping concentrations. The doublet with a higher binding energy (235.5 eV and 232.4 eV for Mo $3d_{3/2}$ and $3d_{5/2}$, respectively) corresponds to the Mo^{+6} oxo-species. On the other hand, the doublet with a lower binding energy (234.6 eV and 230.8 eV for Mo $3d_{3/2}$ and $3d_{5/2}$, respectively) corresponds to the Mo^{+5} oxo-species, which indicates that reduced molybdenum is present in the MTO films. The observed values of the binding energy are consistent with previous reports [26–28]. No Mo^{+4} peak was observed, indicating that the main valences of molybdenum in the sample are +6 and +5. The areas of two doublets increased with increasing Mo doping concentration. The relative intensities of the +5 and +6 oxidation states of molybdenum for all of the samples were approximately 32–35% and 68–70%, respectively. In fact, the spectra of the molybdenum with the +5 oxidation state were significantly enhanced in the annealed films relative to films without annealing because the heat treatment was performed at 600 °C in a reducing gas consisting of 90% N_2 and 10% H_2. In Fig. 6, the binding energies of Ti $2p_{1/2}$ and Ti $2p_{3/2}$ were observed at approximately 464.4 eV and 458.6 eV, respectively, and did not shift to lower values after Mo doping and annealing. This stability suggests that the oxidation state of Ti was primarily +4 [29]. To gain information about the presence of oxygen defects in the

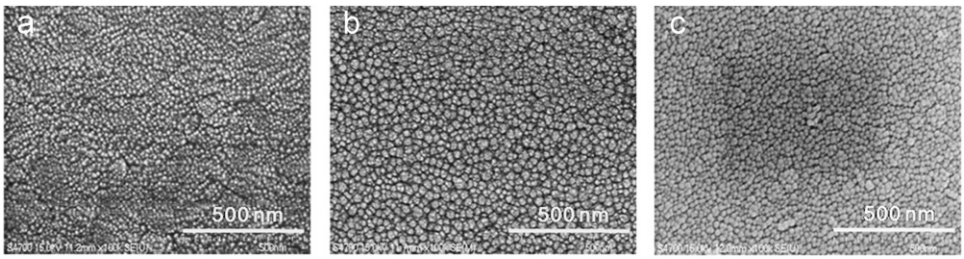

Fig. 4. FESEM photo images of the (a) un-doped, and the TiO_2 films doped with (b) 3 wt% and (c) 10 wt% Mo.

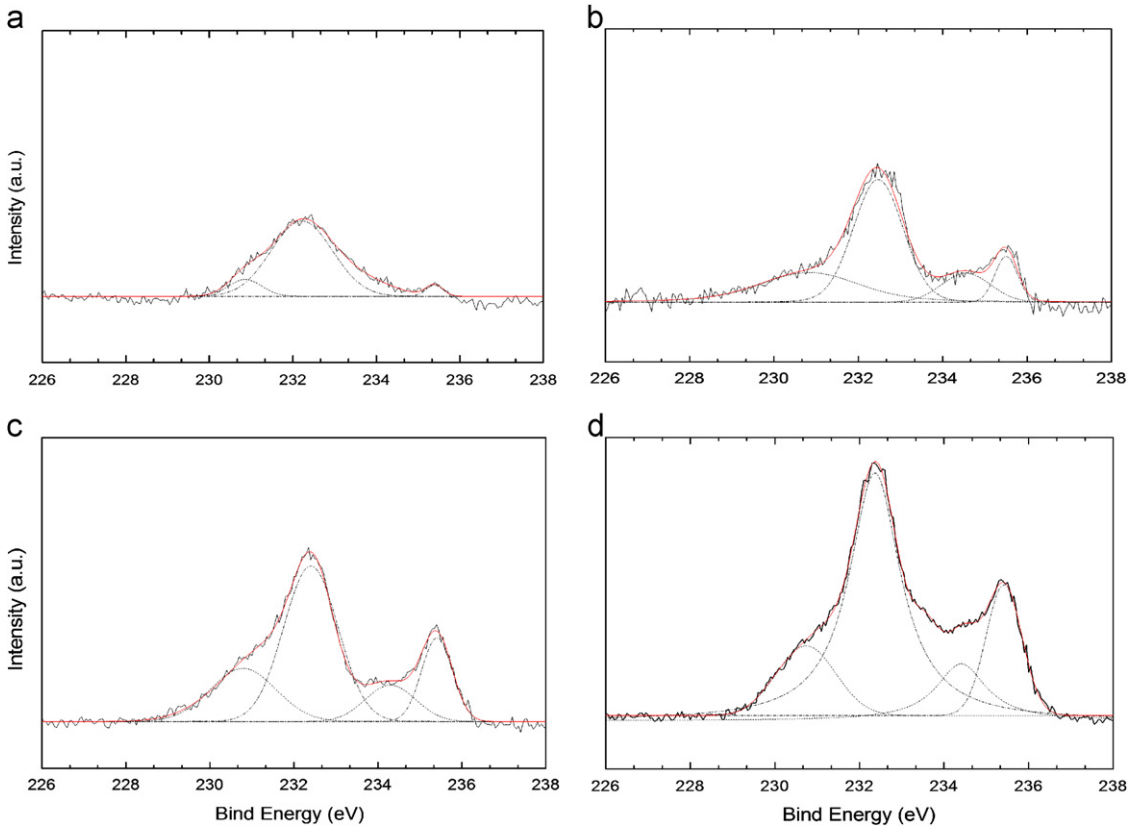

Fig. 5. XPS core level spectra of Mo-doped TiO_2 films for Mo 3d at (a) 3, (b) 5, (c) 7 and (d) 10 wt% Mo doping.

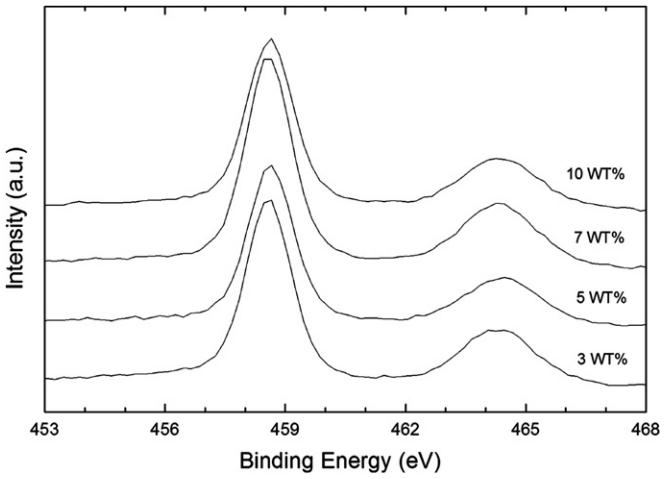

Fig. 6. XPS narrow scan in the Ti 2p region for Mo-doped TiO_2 films at various Mo doping concentrations.

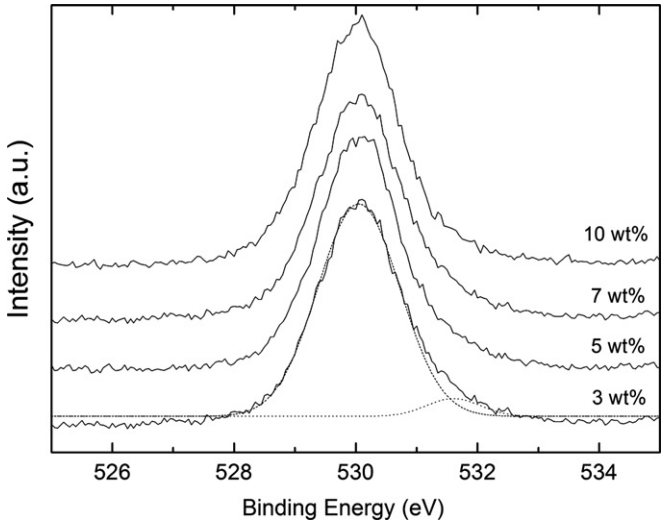

Fig. 7. XPS core level spectra of the O 1 s region for Mo-doped TiO_2 films at various Mo doping concentrations.

deposited films we recorded the O 1s XPS spectra for samples with various Mo doping concentrations. As observed in Fig. 7, the XPS spectra of the O 1s core level are asymmetric, indicating at least two chemical states. After curve fitting, the peak centered at 530.1 eV is attributed to the lattice oxygen of TiO_2, and the other peak at higher binding energy (531.5 eV) can be identified. This peak should be attributed to the O^{2-} ions in the oxygen-deficient regions within the TiO_2 matrix [30].

3.1. Electrical properties

The dependence of the electrical properties of TiO_2 films on the molybdenum doping concentration was measured by the van der Pauw method at room temperature. Fig. 8 shows the typical variation of film resistivity (ρ), carrier density (n), and Hall mobility (μ) as a function of the Mo doping concentration from 0 to 10 wt%. The resistivity of

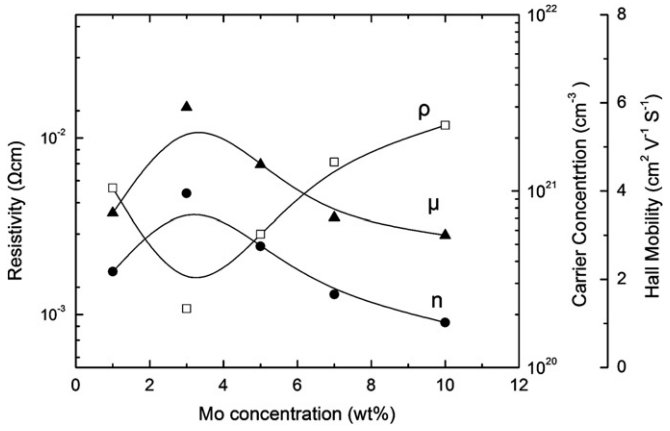

Fig. 8. Electrical resistivity, carrier density and mobility of MTO films as a function of Mo doping concentrations.

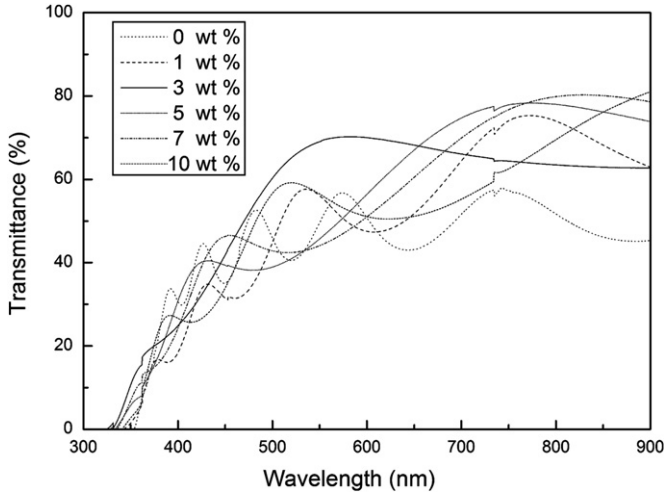

Fig. 9. Optical transmittance spectra of MTO films for different Mo doping concentrations after heat treatment at 600 °C in a reductive atmosphere.

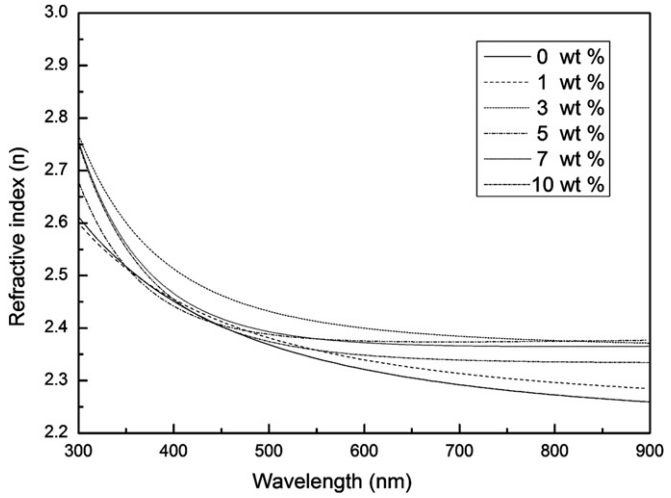

Fig. 10. Refractive index of MTO films for different Mo doping concentrations.

the MTO films was observed to initially decrease with increasing Mo concentrations up to 3 wt%. The carrier density also increased with increasing Mo concentration up to 3 wt%. This initial increase in carrier density resulted in a decrease in the resistivity because of the donor electrons from the Mo dopant. However, after reaching a minimum (at 3 wt% of Mo), the resistivity of the films increased with a further increase in the Mo concentration up to 10 wt% due to an increase in the concentration of the electron traps as a result of excess Mo doping. Above the critical Mo concentration (approximately 3 wt%), excess Mo atoms may occupy interstitial positions which act as carrier traps rather than electron donors [31]. The decrease in carrier density and increase in resistivity beyond 3 wt% Mo is due to the increased disorder of the crystal lattice, which causes phonon and ionized impurity scattering and decrease the mobility [32]. The Mo ion is completed surrounded by TiO_2 before the critical Mo concentration is reached and can act as a donor. However, in an over-doped state, any given Mo ion is affected by other Mo ions due to the excess of Mo. The interaction between Mo ions suppresses their donor ability [33]. This result is also correlated with the loss of crystallinity in MTO films for higher dopant levels as observed in Fig. 2 [34,35]. It also suggested that ITO films with higher doping levels exhibit an increase in resistivity due to an increase in disorder as a result of the decreases in the mobility and free carrier density, which is in agreement with the results shown in Fig. 8. Fig. 8 also shows that the Hall mobility decreased with increasing Mo concentration. The decrease in mobility with increasing Mo dopant concentrations was caused by ionized impurity scattering.

3.2. Optical properties

The transmittance spectra for MTO films deposited at room temperature and annealed at 600 °C with different Mo doping concentrations are displayed in Fig. 9. The average transmittance for all films is approximately 55–65% in the visible part of the spectrum. The major transmission loss is due to reflection because of the high refractive index of TiO_2. The refractive index and extinction coefficient curves for annealed MTO films as a function of wavelength are shown in Figs. 10 and 11. At $\lambda = 550$ nm, the refractive index n ranges from 2.35 to 2.41. The refractive index of the film is related to its density and may be lowered by introducing non-scattering porosity. The porosity and refractive index of MTO films are related by the following equation [36]:

$$P = \left[\frac{1-n^2-1}{n_d^2-1}\right] \times 100\% \quad (2)$$

where n is the refractive index of the porous MTO thin films, and n_d is the refractive index of the pore-free anatase TiO_2 film (n_d=2.52) [37]. The relative porosity and refractive index at 550 nm are shown in Table 1. The film

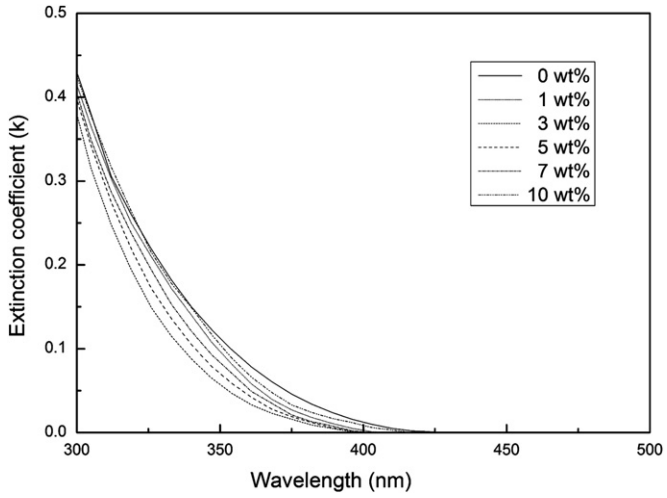

Fig. 11. Extinction coefficients of MTO films for different Mo doping concentrations.

Table 1
Properties of molybdenum-doped TiO_2 films.

Mo doping concentration (wt%)	Transmission at 550 nm (%)	Refractive index at wavelength 550 nm	Porosity ratio (%)	Optical band gap (eV)
0	53	2.34	16.4	3.22
1	56	2.35	15.5	3.31
3	70	2.41	10.1	3.36
5	46	2.37	13.7	3.33
7	45	2.39	12.0	3.32
10	57	2.36	14.6	3.28

doped with 3 wt% Mo has the highest refractive index of 2.41 and that without Mo doping has the lowest value of 2.32. The difference in the magnitude of the crystallization and porosity of the film may explain the differences in the refractive index. As can be observed in the XRD patterns and FESEM images in Figs. 2 and 4, the film doped with 3 wt% Mo exhibited better crystallinity and a denser microstructure, resulting in a higher packing density and thus a higher refractive index. Previous researchers reported that the refractive index of TiO_2 films can be increased by annealing, which enhance crystallization [38,39]. From Fig. 11, all of the films exhibit very low extinction coefficient in the visible region. The extinction coefficient of the un-doped TiO_2 film is greater than those of the MTO films. The high porosity presented as micro-structure defects in un-doped TiO_2 film may contribute to its higher optical absorption.

To evaluate the optical band gap of MTO films, the Tauc model is applied in the high absorbance region of the transmittance spectra [40]. The absorption coefficient, is given by the relation

$$\alpha = \frac{-\ln(T)}{d} \tag{3}$$

where T and d are the transmittance and the film thickness, respectively. The absorption coefficient data were used to determine the energy gap, Eg, by the relation

$$\alpha hv \approx \left(hv - E_g\right)^{1/2} \tag{4}$$

where hv is the photon energy. In this work, the direct band gap of the MTO films was determined by plotting $(\alpha hv)^2$ versus hv and extrapolating the linear regions of the plots to zero absorption. The calculated optical band gaps are listed in Table 1. The direct band gap increased up to 3 wt% MoO_3 and then decreased as MoO_3 concentration approached 10 wt%. This initial increase in the band gap is due to an increase in carrier density as a result of Mo doping. However, above the critical Mo doping, the carrier density decreased with Mo doping due to the crystal disorder caused by excess Mo, which leads the Mo atoms to act as carrier traps instead of electron donors. The apparent band gap widening can be explained by the Burstein–Moss effect [41]. The filling of the electronic states in the conduction band by electron accumulation, resulting from Mo donors, increase the photon energy required for inter-band transitions from the valence band to the higher energy vacant states in the conduction band. This apparent band gap widening corresponding to a blue shift, ΔEg, can also be quantified by the Burstein–Moss formalism

$$\Delta E_g = \frac{h^2}{2m^*}\left(3\pi^2 n_D\right)^{2/3} \tag{5}$$

where h is Plank's normalized constant, m^* is the electron effective mass in the conduction band and n_D is the carrier density. Fig. 12 shows a linear dependence of the optical band gap on $N^{2/3}$. From Fig. 12, an approximately 3.22 eV direct intrinsic absorption edge was obtained by extrapolating N to zero. A blue shift of approximately 0.14 eV is thereby obtained, which is close to the experimental measurements of the band gap for intrinsic absorption edges of anatase TiO_2 films reported in the literature [42–44].

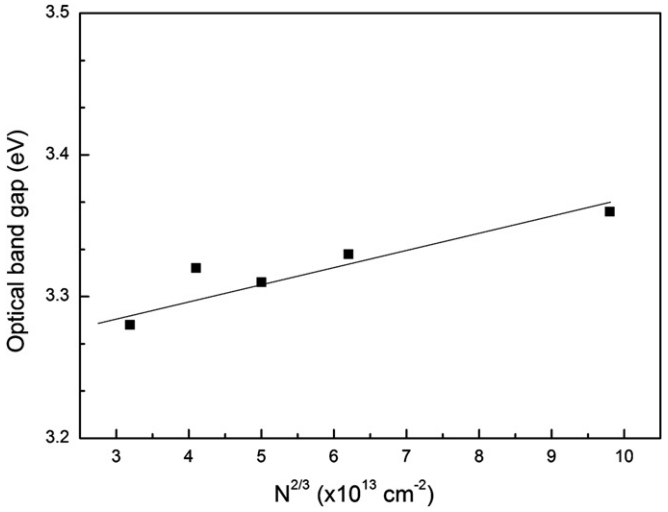

Fig. 12. Optical band gaps as a function of charge carrier density in MTO films.

4. Conclusion

Transparent and conducting TiO_2 thin films doped with molybdenum were produced on glass at room temperature by RF magnetron sputtering. A heat treatment at 600 °C was carried out to the as-deposited films in a reductive atmosphere consisting of 90% N_2 and 10% H_2. The effects of Mo doping concentration on the structural, electrical and optical properties were investigated. The addition of Mo was found to improve the crystallization and increase the grain size of the TiO_2 film. As a result, the TiO_2 film doped with 3 wt% Mo showed an electrical resistivity of $1.1 \times 10^{-3}\,\Omega$ cm with carrier density of $9.7 \times 10^{20}\,cm^{-3}$ and mobility of $5.9\,cm^2/Vs$. XPS was used to identify the chemical composition of the MTO films. The main oxidation states of Mo were +5 and +6 with a peak intensity ratio of approximately 32–35% and 68–70%. In contrast, the binding energy peak of Ti did not shift to a lower oxidation state maintained its +4 oxidation state. The average transmittance of MTO films varied from 55 to 65% in the visible spectrum due to the high reflection of TiO_2. The refractive index of the MTO films ranged from 2.35 to 2.41. The TiO_2 film doped with 3 wt% Mo exhibited a denser microstructure and better crystallinity, producing a higher refractive index and a lower extinguish coefficient. In contrast, the un-doped TiO_2 film presented a more porous microstructure, which lead to a lower refractive index and a higher extinguish coefficient. The optical band gaps of the MTO films were in the range from 3.28 to 3.36 eV for molybdenum doping concentrations between 1 and 10 wt% and greater than that of the un-doped TiO_2 film. A blue shift of 0.14 eV was observed due to the Burstein–Moss effect.

References

[1] Y. Nakato, K. Kai, K. Kawabe, Improvement of characteristics of new-type solar cells, having a transparent conductor/thin SiO_2 layer with ultrafine metal particles as conductive channels/n-Si junction, Solar Energy Materials and Solar Cells 37 (1995) 323–335.

[2] J.R. Bellingham, W.A. Phillips, C.J. Adkins, Intrinsic performance limits in transparent conducting oxides, Journal of Materials Science Letters 11 (1992) 263–265.

[3] T. Minami, S. Takata, T. Kakumu, New multicomponent transparent conducting oxide films for transparent electrodes of flat panel displays, Journal of Vacuum Science and Technology A 14 (1996) 1704–1708.

[4] K. Yanagawa, Y. Ohki, T. Omata, H. Hosono, N. Ueda, H. Kawazoe, Preparation of $Cd_{1-x}Y_xSb_2O_6$ thin film on glass substrate by radio frequency sputtering, Applied Physics Letters 65 (1994) 406–408.

[5] Indium Tin Oxide (ITO) and Replacement Markets: Insight for End Users and Material and Equipment Suppliers, The Information Network, March, 2011.

[6] I. Nakamura, M. Kamiya, I. Takano, Y. Sawada, E. Nakazawa, Formation of In–O Films prepared by the Ar^+ ion reactive assisted deposition method, Surface and Coatings Technology 103–104 (1998) 83–86.

[7] H. Kim, J.S. Horwitz, G. Kushto, A. Pique, Z.H. Kafafi, C.M. Gilmore, D.B. Chrisey, Effect of film thickness on the properties of indium tin oxide thin films, Journal of Applied Physics 88 (2000) 6021–6025.

[8] N. Taga, H. Odaka, Y. Shigesato, I. Yasui, M. Kamei, T.E. Haynes, Electricalproperties of heteroepitaxial grown tindoped indium oxide films, Journal of Applied Physics 80 (1996) 978–984.

[9] A. Salehi, The effects of deposition rate and substrate temperature of ITO thin films on electrical and optical properties, Thin Solid Films 324 (1998) 214–218.

[10] K. Utsumi, O. Matsunaga, T. Takahata, Low resistivity ITO film prepared using the ultra high density ITO target, Thin Solid Films 334 (1998) 30–34.

[11] T. Minami, New n-type transparent conducting oxides, MRS Bulletin 25 (2000) 38–44.

[12] Y. Furubayashi, T. Hitosugi, Y. Yamamoto, K. Inaba, Go Kinoda, Y. Hirose, T. Shimada, T. Hasegawa, Applied Physics Letters 86 (2005) 252101–252103.

[13] H. Tang, H. Berger, P.E. Schmid, F. Levy, Optical properties of anatase (TiO_2), Solid State Communications 92 (1994) 267–271.

[14] E. Yagi, R.R. Hasiguti, M. Aono, Electronic conduction above 4 K of slightly reduced oxygen-deficient rutile TiO_{2-x}, Physical Review B 54 (1996) 7945–7956.

[15] J.W. DeFord, O.W. Johnson, Electron transport properties in rutile from 6 to 40 K, Journal of Applied Physics 54 (1983) 889–897.

[16] L. Forro, O. Chauvet, D. Emin, L. Zuppiroli, H. Berger, F. Levy, High mobility n-type charge carriers in large single crystals of anatase (TiO_2), Journal of Applied Physics 75 (1994) 633–635.

[17] A. Bernasik, M. Radecka, M. Rekas, M. Sloma, Electrical properties of Cr and Nb-doped TiO_2 thin films, Applied Surface Science 66 (1993) 240–245.

[18] T. Hitosugi, Y. Furubayashi, A. Ueda, K. Itabashi, K. Inaba, Y. Hirose, G. Kinoda, Y. Yamamoto, T. Shimada, T. Hasegawa, Ta-doped anatase TiO_2 epitaxial film as transparent conducting oxide, Japanese Journal of Applied Physics 44 (2005) L1063–L1065.

[19] Y. Furubayashi, T. Hitosugi, Y. Yamamoto, Y. Hirose, G. Kinoda, K. Inaba, T. Shimada, T. Hasegawa, Novel transparent conducting oxide: anatase $Ti_{1-x}Nb_xO_2$, Thin Solid Films 496 (2006) 157–159.

[20] T. Hitosugi, A. Ueda, Y. Furubayashi, Y. Hirose, S. Konuma, T. Shimada, T. Hasegawa, Fabrication of TiO_2-based transparent conducting oxide films on glass by pulsed laser deposition, Japanese Journal of Applied Physics 46 (2007) L86–L88.

[21] K. Tonooka, T.W. Chiu, N. Kikuchi, Preparation of transparent conductive TiO2:Nb thin films by pulsed laser deposition, Applied Surface Science 255 (2009) 9695–9698.

[22] T. Hitosugi, N. Yamada, N.L.H. Hoang, J. Kasai, S. Nakao, T. Shimada, T. Hasegawa, Fabrication of TiO_2-based transparent conducting oxide on glass andpolyimide substrates, Thin Solid Films 517 (2009) 3106–3109.

[23] C.J. Tavares, M.V. Castro, E.S. Marins, A.P. Samantilleke, S. Ferdov, L. Rebouta, M. Benelmekki, M.F. Cerqueira, P. Alpuim, E. Xuriguera, J.P. Rivière, D. Eyidi, M.F. Beaufort, A. Mendes, Effect of hot-filament annealing in a hydrogen atmosphere on the electrical and structural properties of Nb-doped TiO_2 sputtered thin films, Thin Solid Films 520 (2012) 2514–2519.

[24] T. Hitosugi, A. Ueda, S. Nakao, N. Yamada, Y. Furubayashi, Y. Hirose, S. Konuma, T. Shimada, T. Hasegawa, Transparent conducting properties of anatase $Ti_{0.94}Nb_{0.06}O_2$ polycrystalline films on glass substrate, Thin Solid Films 516 (2008) 5750–5757.

[25] H. Kim, C.M. Gilmor, Electrical, optical, and structural properties of indium–tin–oxide thin films for organic light-emitting devices, Journal of Applied Physics 86 (1999) 6451–6461.

[26] M.T. Greiner, M.G. Helander, Z.B. Wang, W.M. Tang, J. Qiu, Z.H. Lu, A metallic molybdenum sub-oxide buffer layer for organic electronic devices, Applied Physics Letters 96 (2010) 213302–213304.

[27] F. Werfel, E. Minni, Photoemission study of the electronicstructure of Mo and Mo oxides, Journal of Physics C: Solid State Physics 16 (1983) 6091–6100.

[28] C.D. Wagner, W.M. Riggs, L.E. Davis, J.F. Moulder, G.E. Muilenberg, Handbook of X-Ray Photoelectron Spectroscopy, Perkin–Elmer Corporation, Eden Prairie, MN, USA, 1979.

[29] R. Sanjines, H. Tang, H. Berger, F. Gozzo, G. Margaritondo, F. Lévy, Electronic structure of anatase TiO_2 oxide, Journal of Applied Physics 75 (1994) 2945–2951.
[30] M. Chen, X. Wang, Y.H. Yu, Z.L. Pei, X.D. Bai, C. Sun, R.F. Huang, L.S. Wen, X-ray photoelectron spectroscopy and auger electron spectroscopy studies of Al-doped ZnO films, Applied Surface Science 158 (2000) 134–140.
[31] H.L. Hartnagel, A.L. Dawar, A.K. Jain, C. Jagadish, Semiconducting Transparent Thin Films, Institute of Physics, Bristol, 1995.
[32] M. Mizuhashi, Electrical properties of vacuum-deposited indium oxide and indium tin oxide films, Thin Solid Films 70 (1980) 91–100.
[33] H. Kostlin, R. Jost, W. Kems, Optical and electrical properties of doped In_2O_3 films, Physica Status Solidi A 29 (1975) 87–93.
[34] S.A. Agnihotry, K.K. Saini, T.K. Saxena, K.C. Nagpal, S. Chandra, Studies on e-beam deposited transparent conductive films of In_2O_3:Sn at moderate substrate temperatures, Journal of Physics D: Applied Physics 18 (1985) 2087–2096.
[35] S. Nogichi, H. Sakata, Electrical properties of Sn-doped In_2O_3 prepared by reactive evaporation, Journal of Physics D: Applied Physics 14 (1981) 1523–1529.
[36] B.E. Yoldas, Investigations of porous oxides as an antiflective coating for glass surface, Applied Optics 19 (1980) 14251429.
[37] B.E. Yoldas, P.W. Partlow, Formation of broad band antireflective coating on fused silica for high power laser application, Thin Solid Films 129 (1985) 1–14.
[38] Q. Ye, P.Y. Liu, Z.F. Tang, L. Zhai, Hydrophilic properties of nano-TiO_2 thin films deposited by RF magnetron sputtering, Vacuum 81 (2007) 627–631.
[39] Y.Q. Hou, D.M. Zhuang, G. Zhang, M. Zhao, M.S. Wu, Influence of annealing temperature on the properties of titanium oxide thin film, Applied Surface Science 218 (2003) 98–106.
[40] J. Tauc, R. Grigorovic, A. Vancu, Optical properties and electronic structure of amorphous germanium, Physica Status Solidi 15 (1966) 627–637.
[41] T.S. Moss, Optical Property of Semiconductor, Butterworths, London, 1959.
[42] S.F. Wang, Y.F. Hsu, Y.S. Lee, Microstructure evaluation and optical properties of doped TiO_2 films prepared by RF magnetron sputtering, Ceramics International 32 (2006) 121–125.
[43] W.A. Badway, R.S. Momtaz, E.M. Elgiar, Solid state characteristics of indium-incorporated TiO_2 thin films, Physica Status Solidi 118 (1990) 197–202.
[44] D. Mardare, P. Hones, Optical dispersion analysis of TiO_2 thin films based on variable-angle spectroscopic ellipsometry measurements, Materials Science and Engineering B 68 (1999) 42–47.